Dipole Anisotropy in Gravitational Wave Source Distribution

Gopal Kashyap^a Naveen K. Singh^b Khun Sang Phukon^{c,d,e,f} Sarah Caudill^{c,e,g} Pankaj Jain^b

- ^aDepartment of Physics, School of Advanced Sciences, Vellore Institute of Technology, Vellore, Tamil Nadu 632014, India
- ^bSir P.T. Sarvajanik College of Science, Surat -395001, Gujarat, India
- ^cNikhef National Institute for Subatomic Physics, Science Park, 1098 XG Amsterdam, The Netherlands
- $^d {\rm Institute}$ for High-Energy Physics, University of Amsterdam, Science Park, 1098 XG Amsterdam, The Netherlands
- ^eInstitute for Gravitational and Subatomic Physics, Utrecht University, Princetonplein 1, 3584 CC Utrecht, The Netherlands
- ^fSchool of Physics and Astronomy and Institute for Gravitational Wave Astronomy, University of Birmingham, Edgbaston, Birmingham, B15 9TT, United Kingdom
- ^gDepartment of Physics, University of Massachusetts, Dartmouth, MA 02747, The USA
- ^hDepartment of Space Science & Astronomy, Indian Institute of Technology, Kanpur 208016, India

E-mail: gplkumar87@gmail.com, naveen.nkumars@gmail.com, ksphukon@star.sr.bham.ac.uk, scaudill@umassd.edu, pkjain@iitk.ac.in

Abstract. Our local motion with respect to the cosmic frame of rest is believed to be dominantly responsible for the observed dipole anisotropy in the Cosmic Microwave Background Radiation (CMBR). We study the effect of this motion on the sky distribution of gravitational wave (GW) sources. We determine the resulting dipole anisotropy in GW source number counts, mass weighted number counts, which we refer to as mass intensity, and mean mass per source. The mass M dependence of the number density n(M) distribution of BBH is taken directly from data. We also test the anisotropy in the observable mean mass per source along the direction of the CMB dipole. The current data sample is relatively small and consistent with isotropy. The number of sources required for this test is likely to become available in near future.

\mathbf{C}	ontents	
1	Introduction	1
2	The Effect Of Local Motion on GW Source Distribution	2
3	Generalized Mass Distribution	4
4	Data Analysis	7
5	Conclusions	10

1 Introduction

The standard Λ CDM model of modern cosmology is based on the assumption of isotropy and homogeneity of the Universe at large distance scales, known as the Cosmological Principle. A testable consequence of this would be an isotropic distribution of galaxies at large distance scales. There are many indications that the Universe may be isotropic at scales $\gtrsim 100~\rm Mpc~[1-9]$. The most used source for the measurement of the isotropy of the Universe is the Cosmic Microwave Background Radiation (CMBR). The analysis of CMBR temperature and polarisation fluctuations using Planck observations shows small-scale statistical deviations which are consistent with the cosmological principle. The largest temperature anisotropy in the CMBR is the dipole which is interpreted in terms of our local motion with respect to the CMB rest frame and has been measured in Refs. [2, 8–12]. Considering the dipole as being solely caused by our motion, the velocity is found to be (369.82± 0.11 Km s⁻¹) in the direction, $l = 264.021^{o} \pm 0.011^{o}$, $b = 48.253 \pm 0.0005^{o}$ in galactic coordinates [8, 10, 11]. In J2000 equatorial coordinates, the direction parameters are $RA = 167.9^{o}$, $DEC = -6.93^{o}$.

Our local motion is also expected to generate a dipole anisotropy in the large scale structure [13–15]. Such an anisotropy has been observed in the distribution of radio sources [16–21] and in the diffuse X-ray background [22]. These studies find reasonable agreement with the direction of CMBR dipole. However, surprisingly the dipole amplitude in radio observations is found to be much larger than predicted [18–21]. A strong signal of deviation from the CMB prediction is also seen in the infrared observations [23]. A recent study attributes these deviations, along with the observed Hubble tension, to a large scale inhomogeneity in the Universe, arising due to cosmic super-horizon perturbation modes [24]. While these inferences may be speculative, the observation of gravitational waves provides an independent probe to study the isotropy of the Universe and test these claims.

The detection of gravitational waves by Advanced LIGO [25] and Advanced Virgo [26] detectors revealed the existence of a detectable population of coalescing stellar-mass binary black holes (BBHs). Studies of gravitational wave signals from resolved, well-localized BBH mergers present another tool to probe the anisotropy of the Universe. Advanced LIGO and Advanced Virgo released the details of more than 50 compact binary merger events over the observations of first run (O1), second run (O2) and half of the third run (O3a). These observations are grouped in the gravitational-wave transient catalog GWTC-1 [27], GWTC-2 [28] and GWTC-2.1 [29]. With the completion of the second part of the third observing run (O3b) in the collaboration with LIGO, Virgo and KAGRA (LVK), the total number of

gravitational-wave merger events that includes BBHs, neutron star-black holes (NSBHs) and binary neutron stars (BNS) has been increased to 90. GWTC-3 is the cumulative catalog describing all the gravitational-wave transients found in observing runs upto the end of the third observing run (O3) of LIGO-Virgo detectors[30]. These BBH detections enable determining the astrophysical properties of the BBH population, such as mass and spin distribution of BH populations, the merger rate of such systems and, their evolution across cosmic time [31–33]. Compact binary sources of gravitational wave transient catalog are also used to get some information about the overall sky distribution of events [34, 35]. The sky positions of the GW events are localized by performing coherent analyses of multiple detectors' data using full Bayesian parameter estimation method [36–38] or rapid Bayesian reconstruction method [39]. During O1 and large part of O2 only the two LIGO detectors (HL) network was operational, causing sky localization areas of the sources to be broader in the range of hundreds to thousands square degrees [27, 40]. The addition of Advanced Virgo to the gravitational-wave detectors network during O2 and O3 has yielded many well-localized sources observed by all three detectors of the Advanced LIGO, Virgo (HLV) network with sky areas lesser than 100 square degrees. Such gravitational-wave sources with substantially small areas can be utilized to study the isotropy of the Universe [34, 35, 41-43]. The sky localization areas of sources will improve further during the O4 observation of the Advanced LIGO, Virgo, and KAGRA (HLVK) network [44]. With a future five detectors network including the third LIGO detector in India, a significant fraction of gravitational-wave sources will be localized to few square degrees [45].

In this paper, we determine the dipole anisotropy in the extracted black hole mass distribution arising due to our local motion. We also use LIGO/Virgo data [46] to explore the dipole anisotropy in the distribution of BBH mergers. Such an analysis requires the distribution of number counts per unit mass, which we extract directly from data. We assume a functional form for the distribution law for the total mass of BBH and fit the parameters of the distribution using the data. We determine the expected dipole anisotropy in this mass distribution of BBH caused by our local motion. We also determine the dipole anisotropy in mass intensity and mass per source. Next, we extract sky locations of sources from available posterior distributions of BBH merger events and test the anisotropy in distribution of sources with respect to the CMB direction.

The manuscript is structured as follows. In Sec. 2, we outline the effect of local motion on the observed GW source mass distribution, assuming the power law distribution. We present a generalized mass distribution in Sec. 3 and obtain the fit parameters from the GW data for the various cuts on BBH total mass. We also determine the expected dipole anisotropy in GW sources. In Sec. 4, we investigate the anisotropy in observed BBH event and then we conclude our results in Sec. 5.

2 The Effect Of Local Motion on GW Source Distribution

We start with the assumption that the GW sources are distributed isotropically in the cosmic frame of rest. Our local motion with respect to this frame will introduce two effects, namely, Doppler boosting and wave aberration. The combined effect is expected to change the observed source count and mass intensity (mass weighted number counts) of GW sources in the sky as a function of the sky position.

Consider a binary system of component masses m_1 and m_2 in the comoving frame. The total mass M, chirp mass \mathcal{M}_c and symmetric mass ratio η are defined as $M = m_1 + m_2$,

 $\mathcal{M}_c = M\eta^{3/5}$ and $\eta = m_1m_2/M^2$ respectively. From the observed GW waveform, we can measure the Chirp mass of binary [47],

$$\mathcal{M}_c = \frac{c^3}{G} \left[\frac{5}{96} \pi^{-8/3} \nu_{obs}^{-11/3} \dot{\nu}_{obs} \right]^{3/5}. \tag{2.1}$$

Here, \mathcal{M}_c is the chirp mass observed in the moving local frame and ν_{obs} is the GW frequency in the local frame.

We next determine the anisotropy in the distribution of \mathcal{M}_c generated due to our motion with respect to the cosmic frame of rest. The chirp mass is affected by the relative motion of the detector with respect to the source. However, this effect will maintain the isotropy of this mass distribution in the cosmic frame of rest and the anisotropy will be generated purely due to our motion relative to this frame. Furthermore, the chirp mass \mathcal{M}_c and the total mass M are related by $\mathcal{M}_c = M\eta^{3/5}$, where η depends on the mass ratio m_1/m_2 . Assuming that the mass ratio is distributed isotropically in the cosmic frame of rest, our analysis is also directly applicable to the total mass M.

Due to the Doppler effect, the shift in frequency of GW is given by [13]

$$\nu_{obs} = \nu_{rest} \delta \tag{2.2}$$

where, $\delta \approx (1 + \frac{v}{c}\cos(\theta))$ is the Doppler factor, v is the velocity of observer making an angle θ with the source. As the observed frequency is Doppler shifted, the mass in the rest frame and the moving frame is related by

$$(\nu_{obs}^{-11/3} \dot{\nu}_{obs})^{3/5} = \frac{1}{\delta} (\nu_{rest}^{-11/3} \dot{\nu}_{rest})^{3/5}$$

This leads to,

$$\mathcal{M}_{obs} = \frac{1}{\delta} \mathcal{M}_{rest}, \tag{2.3}$$

where \mathcal{M}_{obs} and \mathcal{M}_{rest} are chirp masses in the local frame and the cosmic rest frame, respectively. Furthermore, the aberration effect changes the solid angle in the direction of motion, i.e., $d\Omega_{obs} = d\Omega_{rest}\delta^{-2}$.

Let us first assume that the number count distribution has a power law BBH total mass M dependence in the cosmic frame of rest, i.e.,

$$\frac{dN}{d\Omega}(M > M_{min}) = kM^{-\alpha}.$$
(2.4)

M will also follow the relation, Eq.(2.3), between rest frame and moving frame. Let us denote the differential number count per unit solid angle per unit mass by $n(\theta, \phi, M)$, where (θ, ϕ) are polar angles corresponding to the direction of observation or sky location of the source. Assuming isotropy, we have, in the rest frame

$$n_{rest}(\theta, \phi, M_{rest}) \equiv \frac{d^2 N_{rest}}{d\Omega_{rest} dM_{rest}} = k\alpha M_{rest}^{-\alpha - 1}.$$
 (2.5)

Let $d^2 N_{obs}$ be the number of sources in bin $d\Omega_{obs} dM_{obs}$ and $d^2 N_{rest}$ be the number of sources in the corresponding bin in the rest frame. We have

$$d^{2} N_{obs} = d^{2} N_{rest} = n_{rest} d\Omega_{rest} dM_{rest}$$
$$= k\alpha M_{rest}^{-\alpha - 1} \delta^{2} d\Omega_{obs} dM_{rest}. \tag{2.6}$$

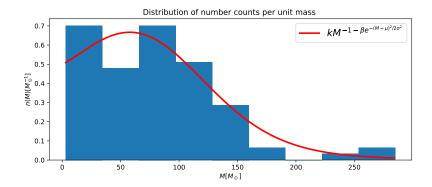


Figure 1. The fit to the distribution of number counts per unit mass, dN/dM, for the functional form given in Eq.(3.1), over the mass range $M > 3M_{\odot}$. The fit parameters are $\beta = -1.072$, $\mu = 51.695M_{\odot}$, $\sigma = -147.71M_{\odot}$.

Using the relation for M_{rest} , we obtain,

$$d^{2}N_{obs} = k\alpha \,\delta^{2-\alpha}M_{obs}^{-\alpha-1}d\Omega_{obs}\,dM_{obs}.$$
(2.7)

Integrating over M from M_{min} to ∞ , we get

$$\frac{dN_{obs}}{d\Omega_{obs}} = k(M_{min})^{-\alpha} \delta^{2-\alpha} = \frac{dN_{rest}}{d\Omega_{rest}} \delta^{2-\alpha}.$$
 (2.8)

Hence, the Doppler boosting and aberration, at leading order, will produce a dipole anisotropy in GW source count, given by

$$\vec{D}_N(v) = [2 - \alpha](\vec{v}/c).$$
 (2.9)

3 Generalized Mass Distribution

Let us generalize the distribution of total mass M of the binary which takes into account the deviation from a pure power law behavior. We assume the following functional form of $n(\theta, \phi, M_{rest})$

$$n(\theta, \phi, M_{rest}) \equiv \frac{d^2 N_{rest}}{d\Omega_{rest} dM_{rest}} = k M_{rest}^{-1 - f(M_{rest})}, \tag{3.1}$$

where,

$$f(M_{rest}) = \beta \exp \left[-\frac{(M_{rest} - \mu)^2}{2\sigma^2} \right].$$

We fit this functional form to the binary mass data, as shown in Fig.1. Here we have used the total masses of binary in the detector frame. We find that our functional form of mass distribution is consistent with the other mass models [48–50].

Following the steps described in Sec. 2, we obtain the generalized form of Eq. (2.7), at leading order in $(v/c)\cos\theta$,

$$d^{2}N_{obs} = kM_{obs}^{-1 - f(M_{obs})} \left[1 - M_{obs} \frac{v}{c} \cos \theta \frac{df(M_{obs})}{dM} \ln(M_{obs}) \right] \delta^{2 - f(M_{obs})} d\Omega_{obs} dM_{obs}.$$
 (3.2)

Integrating M_{obs} from M_{min} to M_{max} , we get

$$\frac{dN_{obs}}{d\Omega_{obs}} = k \left(I_1 + (2I_1 + I_2) \frac{v}{c} \cos \theta \right)
= \frac{dN_{rest}}{d\Omega_{rest}} \left(1 + a \frac{v}{c} \cos \theta \right),$$
(3.3)

where,

$$\frac{dN_{rest}}{d\Omega_{rest}} = kI_1 \tag{3.4}$$

$$a = 2 + \frac{I_2}{I_1} \tag{3.5}$$

$$I_1 = \int_{M_{min}}^{M_{max}} M_{obs}^{-1 - f(M_{obs})} dM_{obs}$$
(3.6)

$$I_2 = -\int_{M_{min}}^{M_{max}} [f(M_{obs}) + M_{obs}f'(M_{obs}) \ln(M_{obs}) M_{obs}^{-1 - f(M_{obs})} dM_{obs}.$$
 (3.7)

If the sources are distributed isotropically in the cosmic rest frame, the observed amplitude of Dipole anisotropy in source counts will be

$$|D_N| = a \frac{v}{c} \cos \theta. \tag{3.8}$$

Integrating I_1 and I_2 from $M_{min}=3M_{\odot}$ to $M_{max}=400M_{\odot}$ and using the fit parameters, we obtain

$$I_1 = 179.3, \quad I_2 = -1.56, \quad a = 1.991$$
 (3.9)

Taking the local velocity to be, v=370 Km/s, we expect that the amplitude of dipole anisotropy will be $|D_N| \approx 2.46 \times 10^{-3}$ for $M > 3M_{\odot}$.

We next generalise this calculation to mass intensity, M_I . This is defined as the number counts weighted by mass, i.e.,

$$d^2M_I = Md^2N. (3.10)$$

We have,

$$d^2 M_{I,obs} = M_{obs} d^2 N_{obs} = M_{obs} n_{rest} d\Omega_{rest} dM_{rest}.$$
(3.11)

Using Eq.(3.2) and integrating over M_{obs} from M_{min} to M_{max} , we obtain

$$\frac{dM_{I,obs}}{d\Omega_{obs}} = \frac{dM_{I,rest}}{d\Omega_{rest}} \left(1 + b \frac{v}{c} \cos \theta \right), \tag{3.12}$$

where,

$$\frac{dM_{I,rest}}{d\Omega_{rest}} = kI_3 \tag{3.13}$$

$$b = 2 + \frac{I_4}{I_3} \tag{3.14}$$

$$I_3 = \int_{M_{min}}^{M_{max}} M_{obs}^{-f(M_{obs})} dM_{obs}$$
(3.15)

$$I_4 = -\int_{M_{min}}^{M_{max}} [f(M_{obs}) + M_{obs}f'(M_{obs}) \ln M_{obs}] M_{obs}^{-f(M_{obs})} dM_{obs}$$
 (3.16)

Therefore, the observed dipole anisotropy in mass intensity is given by

$$D_M = b \frac{v}{c} \cos \theta. \tag{3.17}$$

We also consider another observable, mass per source in angular bin of size $d\Omega$, defined as,

$$\frac{dm}{dN} = \frac{(dM_I/d\Omega)}{(dN/d\Omega)}. (3.18)$$

Using Eq.(3.3) and Eq.(3.12), the observed value of mass per source, at leading order in $(v/c)\cos(\theta)$, is given by

$$\frac{dm_{obs}}{dN_{obs}} = \frac{dm_{rest}}{dN_{rest}} \left(1 - d\frac{v}{c} \cos \theta \right), \tag{3.19}$$

where d = (a - b). Hence, the observed dipole anisotropy in mass per source will be

$$D_m = -d\frac{v}{c}\cos\theta. (3.20)$$

It is quite interesting that the dipole in this parameter is opposite to that in number counts. Hence it may be very useful to test the kinematic origin of the dipole.

$\overline{M(M_{\odot})} >$. 3	10	20	30
β	-1.072	-1.074	-1.106	-1.082
μ	51.695	60.531	27.771	87.903
σ	-147.71	-134.69	-167.52	-78.874
a	1.991	1.95	1.846	1.879
b	1.039	1.028	1.01	0.991
d	0.952	0.922	0.836	0.887

Table 1. The fit parameters corresponding to Eq.(3.1) for various cuts on mass and values of a, b and d for each set of parameters are given.

The fit parameters corresponding to Eq.(3.1) and values of a, b and d are given in Table 1 for different cuts on the mass of binary. We point out that the parameter d is also quite large. This is in contrast to a pure power law, in which case we do not expect any dipole anisotropy in mass per source in analogy to brightness per source in the case of radio data [21]. In comparing with the results of matter dipole [13] we find that the signal in number

counts is reduced by a factor of 2. Hence for a three sigma detection we would require four times as many sources. Using the calculation in [13] we find that this number comes out to be approximately 8×10^5 . This may be within reach of future next generation detectors, such as Einstein Telescope and Cosmic Explorer [51–53]. These detectors might observe $\sim 10^5$ GWs per year coming from BBHs and BNSs mergers with signal to noise ratio threshold more than 9, as discussed in [41]. This number of GWs events are estimated for redshift shell of z=2. Therefore, it may take $\sim 8(2)$ years of observation to detect the $3\sigma(2\sigma)$ level dipole anisotropy in source number counts. In any case, given that this effect will also be observed in galaxy surveys, even a one sigma detection, requiring an order of magnitude fewer sources, would be very useful to establish consistency. We next determine the number of sources needed to observe the dipole in mass per source. This is dependent on the standard deviation in the mass distribution. Given that the velocity is about 370 Km/sec and d=0.95 we expect the dipole amplitude to be approximately 10^{-3} . We find that a three sigma detection in this case requires about 4 million sources. It may take $\sim 40(7)$ years of observation to detect the $3\sigma(2\sigma)$ level dipole anisotropy in mass per source.

4 Data Analysis

The currently available GW data is rather limited and we do not expect to obtain a signal of local velocity in this data. The resulting dipole anisotropy signal is of similar strength as in radio sources and hence we require roughly 8×10^5 sources to extract a signal at 3 sigma significance [13]. However, the required signal is within the reach of gravitational wave detectors in near future. In order to illustrate the procedure we extract the dipole in the mass per source.

The posterior samples containing information about the parameters of events were taken from the LIGO/Virgo data released via the Gravitational-Wave Open Science Center (GWOSC)[46]. We extracted the mass and location of each source using the given probability distribution. For few sources the probability distribution of their sky location (RA, DEC) are uni-modal and are completely in either forward or backward hemisphere with respect to the CMB dipole direction $(RA = 167.9^{\circ}, DEC = -6.93^{\circ})$. Other sources have multi-modal probability distribution of sky location and spread across both the hemispheres. As CMB dipole is near to the Celestial equator, so we assume that the position of any event with respect to the CMB dipole direction will only be decided by the angle RA of that event. To estimate the probability of occurrence of these sources in any one of the hemispheres we use the idea of finite mixture modelling for the probability distribution of RA.

Let f(x) be the probability distribution of RA, we can write it as

$$f(x) = pf_1(x) + (1-p)f_2(x)$$
(4.1)

where we have taken f_1 and f_2 both Gaussian and there would be 5 parameters to estimate from the data, $p, \sigma_1, \sigma_2, \mu_1$, and μ_2 , defined as mixture proportion, the standard deviations and means respectively for the distributions f_1 and f_2 . One such fitting is shown in Fig. [2] for the event GW191219_163120.It may be possible to improve the fit using a different functional form. This may improve the extracted position coordinates of the sources and hence lead to better determination of the dipole. However, the dominant source of error is the intrinsic fluctuations in number counts and the error in mass values or positions is comparatively negligible. Hence, we find that our analysis is sufficiently reliable and postpone further refinements to future research.

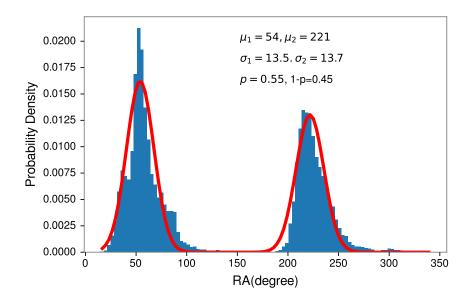


Figure 2. Bimodal probability distribution of RA and approximated Gaussian distributions.

From Fig. [2], we can say that probability of the event at $RA_1 = 54$ is 0.55 and probability of event at $RA_2 = 221$ is 0.45. To get an estimate of the declination angle (DEC) of the event at RA_1 and RA_2 , we look into the skymap of the given event and approximated the corresponding angles as $DEC_1 = -35$ and $DEC_2 = 35$ directly from the given skymap, as shown in Fig. [3]

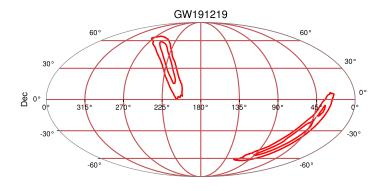


Figure 3. Skymap of the event GW191219_163120

We have done the same analysis for all the events and determine the angles RA, DEC and corresponding probabilities of each event. The resulting skymap of all events weighted with their probability is shown in Fig.[4]. Here colorbar represents the probability of the event.

We determine the cosine of angle $(\cos \theta)$ between unit vector along the CMB dipole and

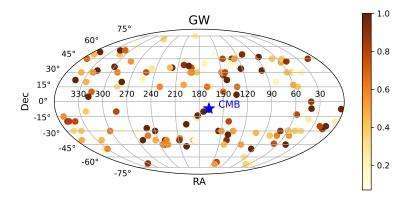


Figure 4. Sky location of all GW events with the colorbar showing their probability at that position.

unit vector along the direction of each source. In forward hemisphere with respect to CMB dipole, $\cos\theta$ will be positive and in backward hemisphere $\cos\theta$ will be negative. We use the masses of events in detector frame. The results are shown in Table 2 .

In order to determine if the sources are distributed isotropically we determine the observable mean value of the mass per source in each hemisphere. We define mean mass per source m as:

$$m = \frac{\sum_{i=1}^{N} M_i p_i}{\sum_{i=1}^{N} p_i} . \tag{4.2}$$

where M_i is the observed mass of the source and p_i the probability that the source lies in a particular hemisphere. From data we find that the mean mass per source in forward hemisphere is $86.19_{2.55}^{5.64}~M_{\odot}$ whereas in backward hemisphere it is $84.6_{3.0}^{8.04}~M_{\odot}$. We find that the difference between the two is not statistically significant and hence the data is consistent with isotropy.

We perform a more detailed analysis by determining the best fit value of the dipole amplitude. We test the following model for the mass distribution on sky,

$$M_{\rm th}(\theta,\phi) = M_0 + \delta M \cos \theta \tag{4.3}$$

where θ is the polar angle in a frame with z-axis pointing along the CMB dipole axis and ϕ being the corresponding azimuthal angle. Here M_0 is the monopole term and δM the dipole amplitude. We determine the two parameters M_0 and δM by minimizing the weighted least square difference. This is defined as

$$\Delta = \frac{\sum_{i=1}^{N} p_i (M_i - M_0 - \delta M \cos \theta)^2}{\sum_{i=1}^{N} p_i}$$
(4.4)

The best fit value of parameters is found to be: $M_0 = 85.3 \ M_{\odot}$ and $\delta M = 6.2 \ M_{\odot}$. We point out that sample has dispersion which is much larger than the error bars on individual masses. Hence we ignore the errors in masses while determining the best fit values. We determine the statistical significance of the dipole by simulations. We generate 100 random samples by randomly permuting the mass values among different sources while keeping their angular positions fixed. We determine the best fit values of each of these samples and find that among these 46 lead to dipole values larger than that of the data sample. Hence we conclude that the data is consistent with isotropy.

5 Conclusions

The search for dipole anisotropy in large scale structures is turning out to be very interesting due to results obtained by radio [18–21] and infrared surveys [23]. Both show a significant deviation from the amplitude expected on the basis of the CMB dipole while the direction is found to be in reasonable agreement. Such a trend has raised the possibility that the Universe might be intrinsically anisotropic and has lead to considerable theoretical effort [54]. The GW observations open up a new and independent domain to test this phenomenon. Here we have determined the signal of dipole anisotropy in the GW observations predicted due to our velocity with respect to the cosmic frame of rest. We considered three different observables, the number counts, the number counts weighted by mass (also called mass intensity) and the mean mass per source. We assume a functional form for the mass dependence of the number count distribution and extract the parameters of this function directly from data. We find that all three observables acquire a significant dipole anisotropy due to our local motion, which can be tested reliably once a sufficiently large sample of GW becomes available.

In order to illustrate our procedure, we have also analysed the available data in order to determine whether the mean mass per source shows any deviation in the two opposite hemispheres in the direction of the CMB dipole. We find that the sample is consistent with isotropy. The data sample is currently very small and considerably more data is required to determine the signal of local motion. The signal is within the reach of future gravitational wave observatories and we look forward to a more detailed study of this phenomenon with future data.

Acknowledgments

We thank Marco Finetti for useful discussions. GK acknowledges the Department of Applied Physics, Gautam Buddha University, Greater Noida for initial support. Naveen K Singh acknowledges the School of Physics and Astronomy, Sun Yat-sen University, Zhuhai Campus, China for the financial support during the initial period of the project. This research has made use of data, software and/or web tools obtained from the Gravitational Wave Open Science Center (https://www.gw-openscience.org/), a service of LIGO Laboratory, the LIGO Scientific Collaboration and the Virgo Collaboration. LIGO Laboratory and Advanced LIGO are funded by the United States National Science Foundation (NSF) as well as the Science and Technology Facilities Council (STFC) of the United Kingdom, the Max-Planck-Society (MPS), and the State of Niedersachsen/Germany for support of the construction of Advanced LIGO and construction and operation of the GEO600 detector. Additional support for

Advanced LIGO was provided by the Australian Research Council. Virgo is funded, through the European Gravitational Observatory (EGO), by the French Centre National de Recherche Scientifique (CNRS), the Italian Istituto Nazionale della Fisica Nucleare (INFN) and the Dutch Nikhef, with contributions by institutions from Belgium, Germany, Greece, Hungary, Ireland, Japan, Monaco, Poland, Portugal, Spain.

Table 2: The masses of GW events in detector frame, extracted location of GW sources, probability(p) of occurance of event in forward hemishpere ($\cos \theta > 0$) or in backward hemisphere ($\cos \theta < 0$), and direction with respect to CMB dipole.

S.No	Event	$\mathbf{M}_{det}(M_{\odot})$	RA(deg)	$\mathrm{DEC}(\mathrm{deg})$	p	$\cos \theta$
1	GW150914_095045	$70.92^4_{-3.57}$	141	-67	1	0.45697237
2	GW151012_095443	$46.4_{-4.5}^{12.4}$	59.3	41	0.51	-0.31812088
3	GW151012_095443	$46.4_{-4.5}^{12.4}$	244	-40	0.49	0.26023751
4	$GW151226_033853$	$23.7^{9.2}_{-1.4}$	53	45	0.4	-0.38085937
5	$GW151226_033853$	$23.7^{9.2}$	208	-38	0.6	0.6726463
6	GW170104_101158	60.4^4	345	-22	0.1	-0.87403264
7	GW170104_101158	60.4^{4}	130	45	0.9	0.46857325
8	GW170608_020116	$19.8^{2.28}_{-0.33}$	122	34	1	0.50525259
9	$GW170729_185629$	123^{21}	302	-69	0.9	-0.13492819
10	$GW170729_185629$	123^{21}	156	50	0.1	0.53195002
11	GW170809_082821	70.66	15	-28	1	-0.72362404
12	GW170814_103043	68.8^{3} ₂	47	-45	1	-0.27515847
13	GW170817	$2.75_{-0.016}^{-3}$	197	-23	1	0.84557982
14	$GW170818_022509$	75.76_{6}^{6}	341	22	1	-0.95894268
15	GW170823_131358	90.8^{11}_{-9}	54	30	0.37	-0.40862792
16	GW170823_131358	90.8_{-9}^{11}	252	-35	0.63	0.15279336
17	GW190403_051519	236.18_{-54}^{40}	334	-50	0.25	-0.52697769
18	GW190403_051519	236.18^{40}	191	35	0.75	0.67876321
19	GW190408_181802	$55.6^{3.42}_{-3.83}$	349	53	1	-0.69366892
20	GW190412	$42.1_{-4.51}^{5.36}$	218	35	1	0.45240024
21	GW190413_052954	90.84_{-13}^{15}	66.3	-44	0.76	-0.05977149
22	$GW190413_052954$	90.84_{-13}^{15}	192	75	0.24	0.11798748
23	GW190413 ₋ 134308	$135_{-17.75}^{17.73} 108.9_{-12.44}^{15.31}$	154	-30	1	0.8948518
24	GW190421_213856	$108.9_{-12.44}^{15.31}$	200	-47	1	0.66175767
25	GW190426_190642	312.16_{-44}^{61}	57	-13	0.8	-0.31791357
26	GW190426_190642	312.16_{-44}^{61}	254	23	0.2	0.01500671
27	GW190503_185404	$91.63_{-12.13}^{11.26}$	95	-50	1	0.280053
28	GW190512_180714	$45.31_{-2.8}^{3.88}$	250	-27	1	0.17634627
29	GW190513_205428	$73.6_{-6.72}^{12.57}$	50	42	0.9	-0.42593418
30	GW190513_205428	$73.6_{-6.72}^{12.57}$	286	-30	0.1	-0.34459989
31	$GW190514_065416$	114.64_{-19}^{20}	60	-30	0.1	-0.2039057

22	CITI OOM LOOM LOOM	11.4.0.420	202	0.0	0.0	0 7 7 0 1 0 0 0 0
32	GW190514_065416	114.64^{20}_{-19}	202	38	0.9	0.57346969
33	GW190517	$85.4_{-7.31}^{9.7}$	233	-45	1	0.38085937
0.4	055101	1540418	0.50	4 =	0.7	0.70447000
34	GW190519_153544	154.84^{18}_{-18}	353	45	0.7	-0.78447906
35	GW190519_153544	154.84^{18}_{-18}	183	-16	0.3	0.95454912
36	GW190521_030229	243.3^{58}_{-36}	352	-40	0.48	-0.68094522
37	GW190521_030229	243.3_{-36}^{58}	192	30	0.52	0.72443384
38	GW190521_074359	92.36^{6}_{-5}	280	20	1	-0.39221934
39	GW190527_092055	84.43 54.92	301	-30	0.64	-0.52708111
40	GW190527_092055	84.4354.92	42	-30	0.36	-0.44377511
41	GW190602_175927	$171.9_{-20.58}^{-10.49}$	71	-35	0.6	-0.02848558
42	GW190602_175927	$171.9^{22.64}_{-20.58}$	81	-35	0.4	0.11318094
43	GW190620 ₋ 030421	140.5^{20}_{-22}	40	-18	0.25	-0.54266686
44	GW190620 ₋ 030421	140.5_{-22}^{-22}	252	30	0.75	0.02804227
45	GW190630 ₋ 185205	69.7^{5}_{-4}	340	-20	0.79	-0.88270748
46	GW190630 ₋ 185205	69.7^{5}_{-4}	166	15	0.21	0.92711366
47	GW190701_203306	$129.64_{-14.75}^{16.61}$	40	-7	1	-0.59054774
48	GW190706_222641	$180.3^{22.4}_{-27.8}$	336	-40	0.08	-0.66654857
49	$GW190706_{-}222641$	$180.3^{22.4}_{-27.8}$	148	27	0.92	0.77690516
50	$GW190707_093326$	$23.36_{-0.69}^{1.54}$	310	50	0.43	-0.59593626
51	$GW190707_093326$	$23.36_{0.69}^{1.54}$	150	-30	0.57	0.87841258
52	GW190708_232457	$37.12^{2.83}_{-1.67}$	350	-30	0.34	-0.79879279
53	GW190708_232457	$37.12^{2.83}_{-1.67}$	170	15	0.66	0.92699685
54	GW190719_215514	91.43_{-15}^{74}	340	-30	0.4	-0.79121117
55	GW190719_215514	91.43_{-15}^{-13}	150	30	0.6	0.75775595
56	GW190720_000836	$25.3_{-1.52}^{4.28}$	300	36	1	-0.6093442
57	GW190725_174728	$21.83_{-1.29}^{1.32}$	284	-10	0.8	-0.40913847
58	GW190725_174728	$21.83_{-1.29}^{9.31}$	81	20	0.2	0.00917921
59	GW190727_060333	$104.61_{-11}^{-1.23}$	352	50	0.46	-0.72888692
60	GW190727_060333	$104.61_{-11}^{\overline{13}}$	142	-70	0.54	0.4187993
61	GW190728_064510	$24_{-0.73}^{5.27}$	315	10	0.7	-0.84177514
62	GW190728_064510	$24_{-0.73}^{-0.73}$	94	-60	0.3	0.24213604
63	GW190731_140936	$109.4_{-14.32}^{14.76}$	66	-70	0.36	0.0433694
64	GW190731_140936	$109.4_{-14.32}^{-14.32}$	188	-40	0.64	0.79168889
65	GW190803_022701	$100_{-11.97}^{-14.32}$	94	32	1	0.16951977
66	GW190805_211137	147.36_{-21}^{21}	350	-20	0.9	-0.89093402
67	GW190805_211137	147.36^{21}_{-21}	146	30	0.1	0.73733111
68	GW190814	$27.21_{-1.32}^{1.44}$	13	-25	1	-0.7637364
69	GW190828_063405	78.57^{6}_{-5}	327	30	0.2	-0.86346248
70	GW190828_063405	78.57^{6}_{-5}	142	-20	0.8	0.88039924
71	GW190828_065509	44^{5}_{-4}	344	35	0.08	-0.8804903
72	GW190828_065509	44^{5}_{-4}	140	-40	0.92	0.74961435
73	GW190928_003309 GW190910_112807	100.83^{9}_{-8}	240	-30	1	0.74901433 0.32456233
	GW190910_112807 GW190915_235702		195	-30 37	1	0.52450255 0.63314856
74	GW190915_255702 GW190916_200658	$78.4^{8.37}_{-7.99}$				
75 76		119.7^{39}_{-22}	352 100	-15 20	0.58	-0.92518688
76	GW190916_200658	119.7^{39}_{-22}	190	30	0.42	0.73620694
77	GW190917 ₋ 114630	$13.52^{3.21}_{-3.3}$	262.5	-40	1	0.01656948

70	CW100004 001046	$15.45^{3.22}_{-0.6}$	122 56	7	1	0.70005027
78 70	GW190924_021846		133.56	7	1	0.79885827 0.96337703
79 80	GW190925_232845 GW190926_050336	11 9	182	-14 20	1	-0.9118678
80	GW190926_050336	94.93_{-13}^{44} 94.93_{-13}^{44}	340 134	30 -30	0.47	0.77388862
81 82	GW190929_012149	94.93_{-13} 144_{-19}^{31}	134 282	-30 42	$0.53 \\ 0.55$	
83		144^{-19}_{-19} 144^{31}_{-19}	102			-0.38196681 0.4076923
	GW190929_012149 GW190930_133541	$23.26_{-0.97}^{10.45}$		-32	0.45	-0.59731342
84		0.01	319	55 70	1	
85	GW191103_012549	$23.47_{-0.68}^{4.58}$	267	70	0.36	-0.1670782
86	GW191103_012549	23.41 -0.68	150	10	0.64	0.9093393
87	GW191105_143521	$22.38_{-0.5}^{2.35} 22.38_{-0.5}^{2.35}$	348	-20	0.82	-0.89155909
88	GW191105_143521	22.30 _{-0.5}	136	40	0.18	0.5680422
89	GW191109_010717	$140.43_{-16.71}^{21.32} 43.36_{-9.88}^{13.45}$	230	-40	1	0.43339286
90	GW191113_071753	$43.30_{-9.88}^{-9.88}$ $43.36_{-9.88}^{13.45}$	55	15	0.4	-0.40434715
91	GW191113_071753		228	-40 40	0.6	0.45663057
92	GW191126_115259	26.54 ^{4.14}	323	-40	0.46	-0.61220318
93	GW191126_115259	$26.54_{-0.9}^{4.14}$	126	45	0.54	0.43714558
94	GW191129_134029	$\frac{20.1}{-0.64}$	330	-50	0.6	-0.51477605
95 oc	GW191129_134029	$20.1^{2.94}_{-0.64}$ $62.76^{10.25}_{-5.32}$	183	30	0.4	0.76968704
96	GW191204_110529	0.02	284	15	0.32	-0.45307229
97	GW191204_110529	$62.76_{-5.32}^{10.25}$	132	15	0.68	0.74549564
98	GW191204_171526	$22.74_{-0.48}^{1.94}$	70	-30	0.9	-0.05783255
99	GW191204_171526	$22.74_{-0.48}^{1.94}$ 58 414.81	209	-30	0.1	0.70816562
100	GW191215_223052	$30.41_{-3.68}$	326	20	0.47	-0.90677818
101	GW191215_223052	$58.41_{-3.68}^{4.81}$	116	-45	0.53	0.51843982
102	GW191216_213338	$^{21.2}$ -0.66	320	32	1	-0.80793859
103	GW191219_163120	$36.03_{-2.61}^{2.22}$	54	-35	0.55	-0.2602422
104	GW191219_163120	$30.03_{-2.61}$	221	35	0.45	0.41903645
105	GW191222_033537	119.21-13	50	30	0.1	-0.46260687
106	GW191222_033537	$119.21_{-13}^{15.78}$	209	-40	0.9	0.65060233
107	GW191230_180458	$145.18^{20.39}_{-18.95}$	59	-30	1	-0.218143
108	GW200112_155838	$79.08_{-5.08}^{6.46}$	291	30	0.61	-0.52981134
109	GW200112_155838	$79.08_{-5.08}^{-3.08}$	50	-30	0.39	-0.34195024
110		$7.83_{-1.78}^{1.85}$	41	0	0.87	-0.59603374
111	GW200115_042309	$7.83_{-1.78}^{1.85}$	266	-30	0.13	-0.06080426
112	GW200128_022011	$116.22_{-13.45}^{17.3}$	61	30	0.43	-0.31024455
113	GW200128_022011	$116.22_{-13.45}^{17.3}$	228	-45	0.57	0.43522604
114	GW200129_065458	$74.61_{-3.83}^{4.45}$	318	5	1	-0.86780468
115	GW200202_154313	$19_{-0.34}^{1.99}$	144	22	1	0.79628983
116	GW200208_130117	$91.43_{-10}^{11.41}$	140	-34	1	0.79479254
117	GW200208_222617	$101.61_{-39.7}^{168.47}$	13	45	0.89	-0.72097287
118	GW200208_222617	$101.61_{-39.7}^{168.47}$	187	-40	0.11	0.79614105
119	GW200209 ₋ 085452	$98.5_{-15.83}^{19.22}$	5	-20	0.21	-0.85032302
120	GW200209_085452	$98.5_{-15.83}^{19.22}$	144	45	0.79	0.5564351
121	GW200210_092254	$32.05_{\substack{-4.72 \ -2.72}}^{7.93}$	322	-10	0.4	-0.85846762
122	GW200210_092254	$32.05_{-4.72}^{7.93}$	190	30	0.6	0.73620694
123	GW200216_220804	$135.12^{30.17}_{-32.22}$	310	55	0.7	-0.5481296
124	GW200216_220804	$135.12_{-32.22}^{30.17}$	246	34	0.3	0.10223177

12	e5 GW200219_094415	$102.51_{-11.92}^{14.11}$	21	-25	0.8	-0.70269259
12	26 GW200219_094415	$102.51_{-11.92}^{14.11}$	172	40	0.2	0.68094522
12	27 GW200220_061928		168	-8	1	0.99982413
12	28 GW200220_124850		59	-30	0.4	-0.218143
12	9 GW200220_124850		230	15	0.6	0.41745519
13	30 GW200224_222234		174.7	-10	1	0.99168784
13	31 GW200225_060421	$41.23_{-4.01}^{2.99}$	300	60	0.07	-0.43725605
13	32 GW200225_060421	$41.23^{2.99}_{-4.01}$	110	50	0.93	0.24665263
13	33 GW200302_015811	$73.7^{14.84}_{-7.94}$	68	45	0.4	-0.20600118
13	34 GW200302_015811	$73.7_{-7.94}^{14.84}$	236	-45	0.6	0.34713249
13	35 GW200306_093714	-12.13	41	30	0.2	-0.57650867
13	36 GW200306_093714	-12.13	145	30	0.8	0.73161338
13	GW200308 ₋ 173609	-100	324	30	0.56	-0.84631105
13	38 GW200308 ₋ 173609	-130	142	-45	0.44	0.71675349
13	39 GW200311 ₋ 115853	$75.89^{6.16}_{-5.66}$	3	-7.5	1	-0.93447092
14	40 GW200316_215756		86.5	47	1	0.01299513
14	41 GW200322_091133	$158.1^{362.84}_{-117.39}$	60	17	0.5	-0.32705584
14	42 GW200322_091133	$158.1^{362.84}_{-117.39}$	200	17	0.5	0.76891174

References

- [1] G.F. Smoot, C.L. Bennett, A. Kogut, E.L. Wright, J. Aymon, N.W. Boggess et al., Structure in the COBE Differential Microwave Radiometer First-Year Maps, The Astrophysical Journal 396 (1992) L1.
- [2] D.J. Fixsen, E.S. Cheng, J.M. Gales, J.C. Mather, R.A. Shafer and E.L. Wright, The Cosmic Microwave Background Spectrum from the Full COBE FIRAS Data Set, The Astrophysical Journal 473 (1996) 576 [astro-ph/9605054].
- [3] K.K. Wu, O. Lahav and M.J. Rees, *The large-scale smoothness of the universe*, *Nature* **397** (1999) 225.
- [4] C. Blake and J. Wall, A velocity dipole in the distribution of radio galaxies, Nature 416 (2002) 150.
- [5] C. Marinoni, J. Bel and A. Buzzi, The scale of cosmic isotropy, Journal of Cosmology and Astroparticle Physics 2012 (2012) 036.
- [6] C. Meegan, G. Fishman, R. Wilson, W. Paciesas, G. Pendleton, J. Horack et al., Spatial distribution of gamma-ray bursts observed by batse, Nature 355 (1992) 143.
- [7] C. Scharf, M. Donahue, G.M. Voit, P. Rosati and M. Postman, Evidence for x-ray emission from a large-scale filament of galaxies?, The Astrophysical Journal 528 (2000) L73.
- [8] P. Collaboration et al., Planck 2018 results. I. Overview and the cosmological legacy of Planck, Astron. Astrophys. **641** (2020) A1 [1807.06205].
- [9] N. Aghanim, C. Armitage-Caplan, M. Arnaud et al., *Planck 2013 results. XXVII. Doppler boosting of the CMB: Eppur si muove, Astron. Astrophys.* **571** (2014) A27.
- [10] A. Kogut, C. Lineweaver, G.F. Smoot et al., Dipole anisotropy in the cobe differential microwave radiometers first-year sky maps, The Astrophysical Journal 419 (1993) 1 [astro-ph/9312056].

- [11] G. Hinshaw, J. Weiland, R. Hill et al., Five-Year Wilkinson Microwave Anisotropy Probe Observations: Data Processing, Sky Maps, and Basic Results, Astrophys. J., Suppl. Ser. 180 (2009) 225 [0803.0732].
- [12] P. Collaboration et al., Planck 2018 results. VII. Isotropy and statistics of the CMB, Astron. Astrophys. 641 (2020) A7.
- [13] G.F.R. Ellis and J.E. Baldwin, On the expected anisotropy of radio source counts, Monthly Notices of the Royal Astronomical Society 206 (1984) 377.
- [14] A. Baleisis, O. Lahav, A.J. Loan and J.V. Wall, Searching for large-scale structure in deep radio surveys, Monthly Notices of the Royal Astronomical Society 297 (1998) 545–558.
- [15] J.J. Condon, W.D. Cotton, E.W. Greisen, Q.F. Yin, R.A. Perley, G.B. Taylor et al., The NRAO VLA sky survey, The Astronomical Journal 115 (1998) 1693.
- [16] C. Blake and J. Wall, A velocity dipole in the distribution of radio galaxies, Nature 416 (2002) 150–152.
- [17] F. Crawford, Detecting the cosmic dipole anisotropy in large-scale radio surveys, The Astrophysical Journal 692 (2009) 887–893.
- [18] A.K. Singal, Large peculiar motion of the solar system from the dipole anisotropy in sky brightness due to distant radio sources, The Astrophysical Journal 742 (2011) L23.
- [19] C. Gibelyou and D. Huterer, Dipoles in the sky, Monthly Notices of the Royal Astronomical Society 427 (2012) 1994–2021.
- [20] M. Rubart and D.J. Schwarz, Cosmic radio dipole from nvss and wenss, Astronomy and Astrophysics 555 (2013) A117.
- [21] P. Tiwari, R. Kothari, A. Naskar, S. Nadkarni-Ghosh and P. Jain, Dipole anisotropy in sky brightness and source count distribution in radio nvss data, Astroparticle Physics 61 (2015) 1.
- [22] S.P. Boughn, R.G. Crittenden and G.P. Koehrsen, The large-scale structure of the x-ray background and its cosmological implications, The Astrophysical Journal 580 (2002) 672.
- [23] N.J. Secrest, S. von Hausegger, M. Rameez, R. Mohayaee, S. Sarkar and J. Colin, A Test of the Cosmological Principle with Quasars, Astrophys. J. Lett. 908 (2021) L51 [2009.14826].
- [24] P. Tiwari, R. Kothari and P. Jain, Superhorizon Perturbations: A Possible Explanation of the Hubble-Lemaître Tension and the Large-scale Anisotropy of the Universe, Astrophys. J. Lett. 924 (2022) L36 [2111.02685].
- [25] J. Aasi, B.P. Abbott, R. Abbott, T. Abbott, M.R. Abernathy, K. Ackley et al., Advanced ligo, Classical and Quantum Gravity 32 (2015) 074001.
- [26] F. Acernese, M. Agathos, K. Agatsuma, D. Aisa, N. Allemandou, A. Allocca et al., Advanced virgo: a second-generation interferometric gravitational wave detector, Classical and Quantum Gravity 32 (2014) 024001.
- [27] LIGO SCIENTIFIC COLLABORATION AND VIRGO COLLABORATION collaboration, Gwtc-1: A gravitational-wave transient catalog of compact binary mergers observed by ligo and virgo during the first and second observing runs, Phys. Rev. X 9 (2019) 031040.
- [28] LIGO SCIENTIFIC, VIRGO collaboration, GWTC-2: Compact Binary Coalescences Observed by LIGO and Virgo During the First Half of the Third Observing Run, Phys. Rev. X 11 (2021) 021053 [2010.14527].
- [29] LIGO SCIENTIFIC, VIRGO collaboration, GWTC-2.1: Deep Extended Catalog of Compact Binary Coalescences Observed by LIGO and Virgo During the First Half of the Third Observing Run, 2108.01045.
- [30] LIGO SCIENTIFIC, VIRGO, KAGRA collaboration, GWTC-3: Compact Binary Coalescences Observed by LIGO and Virgo During the Second Part of the Third Observing Run, 2111.03606.

- [31] LIGO SCIENTIFIC, VIRGO collaboration, Binary Black Hole Population Properties Inferred from the First and Second Observing Runs of Advanced LIGO and Advanced Virgo, Astrophys. J. Lett. 882 (2019) L24 [1811.12940].
- [32] LIGO SCIENTIFIC, VIRGO collaboration, Population Properties of Compact Objects from the Second LIGO-Virgo Gravitational-Wave Transient Catalog, Astrophys. J. Lett. 913 (2021) L7 [2010.14533].
- [33] LIGO SCIENTIFIC, VIRGO, KAGRA collaboration, The population of merging compact binaries inferred using gravitational waves through GWTC-3, 2111.03634.
- [34] E. Payne, S. Banagiri, P. Lasky and E. Thrane, Searching for anisotropy in the distribution of binary black hole mergers, Phys. Rev. D 102 (2020) 102004 [2006.11957].
- [35] R. Stiskalek, J. Veitch and C. Messenger, Are stellar-mass binary black hole mergers isotropically distributed?, Monthly Notices of the Royal Astronomical Society **501** (2020) 970–977.
- [36] J. Veitch et al., Parameter estimation for compact binaries with ground-based gravitational-wave observations using the LALInference software library, Phys. Rev. D 91 (2015) 042003 [1409.7215].
- [37] G. Ashton, M. Hübner, P.D. Lasky, C. Talbot, K. Ackley, S. Biscoveanu et al., BILBY: A User-friendly Bayesian Inference Library for Gravitational-wave Astronomy, The Astrophysical Journal Suppl. Ser. 241 (2019) 27 [1811.02042].
- [38] I.M. Romero-Shaw, C. Talbot, S. Biscoveanu, V. D'Emilio, G. Ashton, C.P.L. Berry et al., Bayesian inference for compact binary coalescences with BILBY: validation and application to the first LIGO-Virgo gravitational-wave transient catalogue, MNRAS 499 (2020) 3295 [2006.00714].
- [39] L.P. Singer and L.R. Price, Rapid Bayesian position reconstruction for gravitational-wave transients, Phys. Rev. D 93 (2016) 024013 [1508.03634].
- [40] LIGO SCIENTIFIC, VIRGO collaboration, Binary Black Hole Mergers in the first Advanced LIGO Observing Run, Phys. Rev. X 6 (2016) 041015 [1606.04856].
- [41] S. Mastrogiovanni, C. Bonvin, G. Cusin and S. Foffa, Detection and estimation of the cosmic dipole with the einstein telescope and cosmic explorer, 2209.11658.
- [42] R. Essick, W.M. Farr, M. Fishbach, D.E. Holz and E. Katsavounidis, *An isotropy measurement with gravitational wave observations*, 2207.05792.
- [43] M. Cavaglia and A. Modi, Two-dimensional correlation function of binary black hole coalescences, Universe 6 (2020) 93 [2005.06004].
- [44] KAGRA, LIGO SCIENTIFIC, VIRGO, VIRGO collaboration, Prospects for observing and localizing gravitational-wave transients with Advanced LIGO, Advanced Virgo and KAGRA, Living Rev. Rel. 21 (2018) 3 [1304.0670].
- [45] M. Saleem et al., The science case for LIGO-India, Class. Quant. Grav. 39 (2022) 025004 [2105.01716].
- [46] LIGO SCIENTIFIC, VIRGO collaboration, Open data from the first and second observing runs of Advanced LIGO and Advanced Virgo, SoftwareX 13 (2021i) 100658 [1912.11716].
- [47] LIGO SCIENTIFIC COLLABORATION AND VIRGO COLLABORATION collaboration, Observation of gravitational waves from a binary black hole merger, Phys. Rev. Lett. 116 (2016) 061102.
- [48] C. Talbot and E. Thrane, Measuring the Binary Black Hole Mass Spectrum with an Astrophysically Motivated Parameterization, The Astrophysical Journal 856 (2018) 173 [1801.02699].

- [49] N. Farrow, X.-J. Zhu and E. Thrane, The mass distribution of galactic double neutron stars, The Astrophysical Journal 876 (2019) 18.
- [50] M. Fishbach, R. Essick and D.E. Holz, Does matter matter? using the mass distribution to distinguish neutron stars and black holes, The Astrophysical Journal Letters 899 (2020) L8.
- [51] D. Reitze, R.X. Adhikari, S. Ballmer, B. Barish, L. Barsotti, G. Billingsley et al., *Cosmic explorer: The us contribution to gravitational-wave astronomy beyond ligo*, 1907.04833.
- [52] M. Punturo, M. Abernathy, F. Acernese, B. Allen, N. Andersson, K. Arun et al., The einstein telescope: a third-generation gravitational wave observatory, Classical and Quantum Gravity 27 (2010) 194002.
- [53] S. Dwyer, D. Sigg, S.W. Ballmer, L. Barsotti, N. Mavalvala and M. Evans, Gravitational wave detector with cosmological reach, Phys. Rev. D 91 (2015) 082001.
- [54] L. Perivolaropoulos and F. Skara, Challenges for ΛCDM: An update, 2105.05208.